BMC Genomics

RESEARCH

Open Access

Comparative genome-wide identification and characterization of SET domain-containing and JmjC domain-containing proteins in piroplasms

Qindong Liang[1,2†], Shangdi Zhang[1†], Zeen Liu[2], Jinming Wang[2,3], Hong Yin[2,4*†], Guiquan Guan[2,3*†] and Chongge You[1*†]

Abstract

Background SET domain-containing histone lysine methyltransferases (HKMTs) and JmjC domain-containing histone demethylases (JHDMs) are essential for maintaining dynamic changes in histone methylation across parasite development and infection. However, information on the HKMTs and JHDMs in human pathogenic piroplasms, such as *Babesia duncani* and *Babesia microti*, and in veterinary important pathogens, including *Babesia bigemina*, *Babesia bovis*, *Theileria annulata* and *Theileria parva*, is limited.

Results A total of 38 putative KMTs and eight JHDMs were identified using a comparative genomics approach. Phylogenetic analysis revealed that the putative KMTs can be divided into eight subgroups, while the JHDMs belong to the JARID subfamily, except for BdJmjC1 (BdWA1_000016) and TpJmjC1 (Tp Muguga_02g00471) which cluster with JmjC domain only subfamily members. The motifs of SET and JmjC domains are highly conserved among piroplasm species. Interspecies collinearity analysis provided insight into the evolutionary duplication events of some SET domain and JmjC domain gene families. Moreover, relative gene expression analysis by RT–qPCR demonstrated that the putative KMT and JHDM gene families were differentially expressed in different intraerythrocytic developmental stages of *B. duncani*, suggesting their role in Apicomplexa parasite development.

Conclusions Our study provides a theoretical foundation and guidance for understanding the basic characteristics of several important piroplasm KMT and JHDM families and their biological roles in parasite differentiation.

Keywords Babesiosis, Piroplasm, SET domain, JmjC domain, Methyltransferase, Demethylase, RT–qPCR

†Qindong Liang and Shangdi Zhang contributed equally to this work.

†Hong Yin, Guiguan Guan and Chongge You contributed equally to this work and share last authorship.

*Correspondence:
Hong Yin
yinhong@caas.cn
Guiquan Guan
guanguiquan@caas.cn
Chongge You
youchg@lzu.edu.cn
[1] Laboratory Medicine Center, The Second Hospital & Clinical Medical School, Lanzhou University, Lanzhou, Gansu 730030, P. R. China
[2] State Key Laboratory of Veterinary Etiological Biology, Key Laboratory of Veterinary Parasitology of Gansu Province, Lanzhou Veterinary Research Institute, Chinese Academy of Agricultural Science, Lanzhou, Gansu 730046, P. R. China
[3] State Key Laboratory for Animal Disease Control and Prevention, College of Veterinary Medicine, Lanzhou University, Lanzhou Veterinary Research Institute, Chinese Academy of Agricultural Sciences, Lanzhou, Gansu 730000, P. R. China
[4] Jiangsu Co-Innovation Center for the Prevention and Control of Important Animal Infectious Disease and Zoonose, Yangzhou University, Yangzhou 225009, P. R. China

Background

Piroplasmosis is a group of human and veterinary tick-borne diseases caused mainly by parasites belonging to two Apicomplexa genera, *Babesia* and *Theileria* [1]. *Theileria* parasites, which can infect a number of domesticated and wild ruminants around the world, kill millions of cattle each year and cause enormous economic losses to the livestock industry; of these, *Theileria annulata* and *Theileria parva* are the most common pathogens, while *Babesia* can infect a range of warm-blooded vertebrates, including humans and wild and domestic animals [2, 3]. Human babesiosis is a malaria-like disease caused by a wide spectrum of *Babesia* species, such as *Babesia microti* [4], *Babesia duncani* [5], *Babesia divergens* [6], *Babesia motasi*, [7] *Babesia crassa* [8], *Babesia bigemina* [9], *Babesia venatorum* [10] and *Babesia bovis* [11]. Among these species, *B. microti* is the most common causative agent [12], while *B. duncani* is a highly virulent zoonotic pathogen that can cause severe to fatal infections in laboratory mice and hamsters. In humans, symptoms of *B. duncani* infection range from asymptomatic to mild flu-like illness, and even to fatal, particularly in the elderly, post-splenectomy or immunocompromised individuals [13]. *B. duncani* and *B. microti* pose health threats to humans, domestic and wild animals [14, 15]. *B. duncani* has been found in bighorn sheep and mule deer [16]. Also, *B. microti* has been detected in domestic cats [17] and dogs [18], and small mammals [19, 20] and baboons [21]. Currently, there is a lack of specific drugs or vaccines to treat piroplasm infections, making it urgent to develop effective therapeutic strategies to improve the management of these parasites.

In Apicomplexa parasites, histone lysine methylation levels are associated with parasite virulence [22], motility [23], stage transition [24] and host-parasite interactions [25]. In addition, many key enzymes downstream of histone lysine methylation pathways have been proven to be ideal targets for cancer drug development [26–29]. Intriguingly, several studies have demonstrated that methyltransferase inhibitors show promise as therapeutic drugs for treating malaria parasites [30, 31], *Trypanosoma brucei* [32, 33] and *Leishmania* [34]. Currently, SET (Su(var)3–9, E(z), Trithorax) domain-containing histone lysine methyltransferases (HKMTs) and JmjC (Jumonji C) domain-containing histone demethylases (JHDMs) have been identified and characterized at the genome-wide level in several Apicomplexa parasites, such as *Plasmodium falciparum* [35], *Cryptosporidium parvum* [25] and *Toxoplasma gondii* [36]. The SET domain, a sequence of about 130 amino acid residues first discovered in the *Drosophila* genome, is the enzymatic activity domain of HKMTs and is highly evolutionarily conserved [37, 38], while, the evolutionarily highly conserved JmjC domain is the functionally active region of the JHDM family [39]. Based on sequence similarity and substrate specificity, SET domain-containing HKMTs can be classified into several subfamilies: SETD1, SETD2, SUV3D9, SMYD, SET7/9 and SETD8 [40], and JHDM can be divided into JHDM1, PHF2/PHF8, JARID, JHDM3/JMJD2, UTX/UTY, JHDM2 and JmjC domain only groups [41]. However, little is known about the classification, structural and physical characteristics, and function of HKMTs and JHDMs in human pathogenic babesia, including *B. duncani*, *B. microti*, and in veterinary important pathogens, such as *B. bigemina*, *B. bovis*, *T. annulata* and *T. parva*.

Here, we conducted systematic and comprehensive research on putative KMT and JHDM genes in several representative piroplasm genomes to disclose the information focusing on their physicochemical properties, chromosome distribution, phylogenetic classification and interspecies collinearity. Furthermore, the expression profiles of the retrieved genes at different developmental stages of *B. duncani* were determined by real-time quantitative PCR. Our study will provide the scientific community with new viewpoints and clues to better understand HKMTs and JHDMs and pave the way for research on the role of these methylation regulators in the intraerythrocytic development of human pathogenic and veterinary important piroplasm parasites.

Results

Identification and characterization of the putative KMTs and JHDMs in *B. duncani*, *B. bigemina*, *B. microti*, *B. bovis*, *T. annulata* and *T. parva*

By thoroughly searching the *B. duncani*, *B. bigemina*, *B. microti*, *B. bovis*, *T. annulata* and *T. parva* reference genomes with the SET domain sequences of several well-studied HKMTs, 49 putative SET domain-containing candidates were obtained. However, further structure verification analysis with SMART revealed that 11 hits (GenBank ID: KAK2185947, KAK2197250, XP_001610401, BAN65725, XP_001611356, XP_012768058, XP_952658, XP_954450, XP_955402, XP_061162069 and XP_765804) did not possess any SET domain (data not shown). Consequently, 38 putative KMTs were retrieved from the six genomes. The physicochemical properties including the length of the primary sequence, molecular weight, isoelectric point and subcellular localization are listed in Table 1. The molecular weights of the identified putative KMTs varied from 11.03 kDa (BdSET3) to 549.87 kDa (BbSET1); while, the isoelectric points (PIs) of the 38 putative KMTs fluctuated between 4.43 and 9.04. This finding suggested that the KMT family members of these six species are quite different from each other. Moreover, although the subcellular localization of these 38 putative KMTs varied greatly, the same subfamilies had similar

Table 1 Putative SET domain-containing lysine methyltransferases identified in *Babesia duncani*, *Babesia microti*, *Babesia bigemina*, *Babesia bovis*, *Theileria annulata* and *Theileria parva*

Organism	Name	Subfamily	Locus tag	ORF/bp	GenBank ID	Length/aa	MW/kDa	PI	Subcellular location
B. duncani	BdSET1	SETD1	BdWA1_001603	8937	KAK2196360	2978	339.46	8.78	N
	BdSET2	SETD2	BdWA1_001597	2859	KAK2196354	952	108.56	8.51	C & N
	BdSET3	SUV39	BdWA1_002813	297	KAK2196213	98	11.03	4.43	C & N & E
	BdSET4	LSMT	BdWA1_002728	2508	KAK2196128	835	96.32	5.76	C & N
	BdSET5	SMYD	BdWA1_002381	1476	KAK2195787	491	55.77	4.99	C & N
	BdSET8	SETD8	BdWA1_000254	2577	KAK2197255	858	97.86	6.48	N
B. microti	BmSET1	SETD1	BmR1_04g06700	6477	XP_021337754	2158	236.65	8.85	C & N
	BmSET2	SETD2	BmR1_04g06675	3048	XP_012649939	1015	116.33	8.53	N
	BmSET3	SUV39	BmR1_01G01675	2430	XP_021337406	809	93.53	5.94	C & N
	BmSET5	SMYD	BmR1_03g03600	1449	XP_021338726	482	55.14	5.55	C
	BmSET6	Other	BmR1_03g02355	1788	XP_021338606	595	68.29	5.66	C & N
	BmSET7	SET7/9	BmR1_01G02770	1143	XP_012647617	380	43.30	8.92	C
	BmSET8	SETD8	BmR1_02g00765	2202	XP_021338053	733	83.78	6.20	N
B. bigemina	BbSET1	SETD1	BBBOND_0312510	14,961	XP_012769534	4986	549.87	5.88	N
	BbSET2	SETD2	BBBOND_0312650	5502	XP_012769548	1833	197.88	8.94	C & N
	BbSET3	SUV39	BBBOND_0404490	2511	XP_012770147	836	95.78	6.02	C & N
	BbSET4	LSMT	BBBOND_0405480	3069	XP_012770250	1022	113.09	5.60	C
	BbSET5	SMYD	BBBOND_0108570	1461	XP_012766745	486	55.04	5.14	C
	BbSET6	Other	BBBOND_0308060	2658	XP_012769088	885	98.79	5.06	N
	BbSET7	SET7/9	BBBOND_0302680	2412	XP_012768550	803	89.85	5.53	N
	BbSET8	SETD8	BBBOND_0210330	2646	XP_012768066	881	98.94	5.37	N
B. bovis	BBOVSET2	SETD2	BBOV_III009070	4362	XP_001612032	1453	162.29	7.24	N
	BBOVSET3	SUV39	BBOV_IV002320	2424	XP_001609397	807	91.94	5.84	C & N
	BBOVSET4	LSMT	BBOV_IV001550	2580	XP_001609320	859	98.12	5.89	C
	BBOVSET5	SMYD	BBOV_IV010830	1476	XP_001611004	491	56.23	4.90	C
	BBOVSET6	Other	BBOV_III006000	2865	XP_001611729	954	108.75	5.30	C & N
	BBOVSET7	SET7/9	BBOV_III001355	1221	XP_051623774	406	46.85	5.12	C
	BBOVSET8	SETD8	BBOV_IV004680	2658	XP_001610397	885	100.89	9.04	N
T. annulata	TaSETup1	SMYD	TA06820	1473	XP_954031	490	56.81	4.88	C
	TaSETup2	SETD8	TA21435	2532	XP_954446	843	96.98	6.20	C & N
	TaSETup3	SETD2	TA09850	3252	XP_953444	1083	122.38	6.53	N
	TaSETup4	LSMT	TA05190	4128	XP_955248	1375	159.46	5.52	C & N
	TaSETup5	SETD1	TA09890	10,788	XP_953437	3595	415.35	5.66	N
T. parva	TpSET1	SETD1	TpMuguga_04g02605	11,349	XP_061161906	3782	434.48	6.43	N
	TpSET2	SETD2	TpMuguga_04g02235	3597	XP_764449	1198	136.32	6.37	N
	TpSET4	LSMT	TpMuguga_03g00553	2205	XP_061161062	734	83.67	5.4	C & N
	TpSET5	SMYD	TpMuguga_01g00746	1473	XP_061161629	490	56.77	4.96	C
	TpSET8	SETD8	TpMuguga_01g00281	2535	XP_765808	844	97.56	5.69	C & N

ORF Open reading frame, *PI* isoelectric point, *C* Cytoplasmic, *E* Extracellular, *N* Nuclear

subcellular localization, and most of them had nuclear localization (Table 1).

Additionally, we identified eight putative JHDMs through systematic BLASTp in the six piroplasm genomes with a series of JmjC domain sequences from representative human JHDMs. On the basis of prediction analysis via the ExPASy website, the molecular weights of these JHDMs vary from 33.86 kDa to 84.5 kDa; while, the PIs of these six putative JHDMs are also different from each other (the PI ranges between 5.48 and 8.29). All the putative JHDMs have nuclear localization (Table 2).

Phylogenetic analysis

To analyze the phylogenetic relationships between the putative KMTs of the six species and several well-known HKMTs from *Homo sapiens*, *Drosophila*

Table 2 Putative JmjC domain-containing histone demethylases identified in *Babesia duncani*, *Babesia microti*, *Babesia bigemina*, *Babesia bovis*, *Theileria annulata* and *Theileria parva*

Organism	Name	Subfamily	Locus tag	ORF/bp	GenBank ID	Length/aa	MW/kDa	PI	Subcellular location
B. duncani	BdJmjC1	JmjC domain only	BdWA1_000016	906	KAK2197022	301	33.86	6.41	N
	BdJmjC2	JARID	BdWA1_000055	1494	KAK2197060	497	56.06	6.36	N
B. microti	BmJmjC1	JARID	BMR1_02g02515	1884	XP_012648268	627	71.76	8.22	N
B. bigemina	BbJmjC1	JARID	BBBOND_0403490	2232	XP_012770047	743	84.23	5.48	N
B. bovis	BBOVJmjC1	JARID	BBOV_IV000510	2229	XP_051623027	742	84.50	5.52	C & N
T. annulata	TaJmjC2	JARID	TA19925	2130	XP_954636	709	81.71	8.06	N
T. parva	TpJmjC1	JmjC domain only	TpMuguga_02g00471	975	XP_765037	324	36.99	6.07	N
	TpJmjC2	JARID	TpMuguga_01g02310	2127	XP_061161929	708	81.64	8.29	N

ORF Open reading frame, *PI* isoelectric point, *C* Cytoplasmic, *N* Nuclear

melanogaster and other Apicomplexa species, a phylogenetic tree was constructed from the SET domain amino acid sequences of these proteins by the maximum likelihood ratio method using MEGA 7.0. As shown in Fig. 1A, the 38 putative KMTs were divided into eight KMT subfamilies. However, BmSET6, BdSET6 and BBOVSET6 clustered together to form a new clade distinct from other known HKMTs, suggesting that these three putative KMTs may be parasite-specific enzymes involved in regulating some of the parasite's unique biological processes. Moreover, a phylogenetic cladogram of the JmjC domain proteins was also generated by MEGA 7.0 based on the maximum likelihood ratio algorithm with the JmjC domain protein sequences of the JHDMs of *H. sapiens* and *T. gondii* to examine the evolutionary history of these proteins. Of note, the identified JHDMs were divided into two main subfamilies on the basis of their branching features and bootstrap values. As depicted in Fig. 1B, BdJmjC1 and TpJmjC1 were classified into JmjC domain only subgroup, while the remaining JHDMs were assigned to the JARID subfamily.

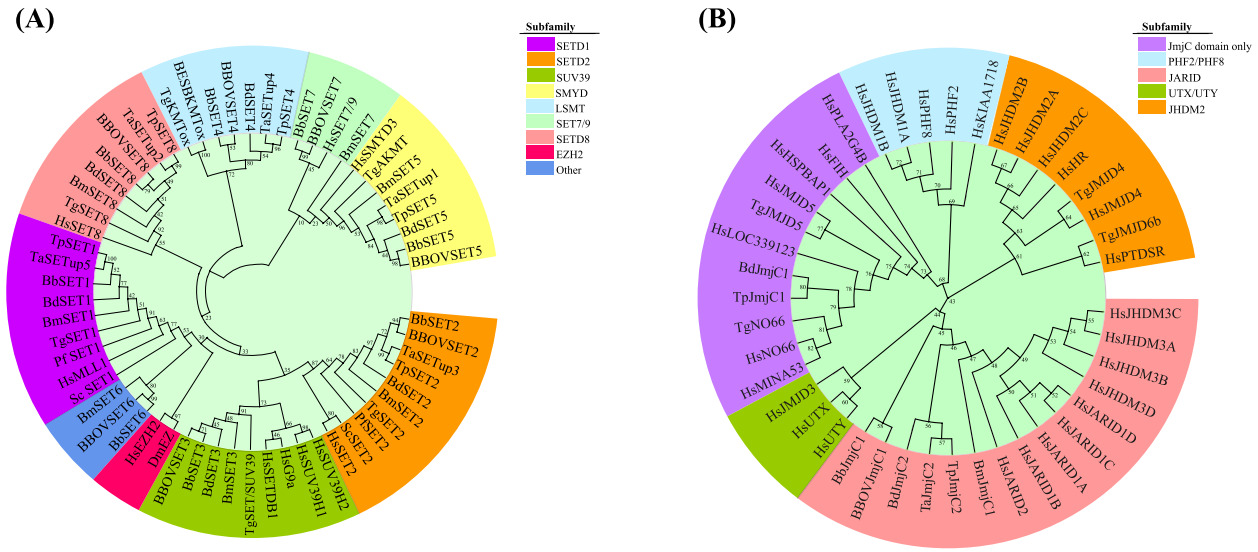

Fig. 1 Phylogenetic trees of the SET domain sequences of the putative KMTs (**A**) and the JmjC domain sequences of the JHDMs (**B**). The SET domain sequences of the KMTs and the JmjC domain sequences of the JHDMs were aligned by Clustal W algorithm, and phylogenetic tree files were generated by MEGA 7.0 by the maximum-likelihood method and visualized by R software. The numbers at each branch point on the evolutionary trees represent the bootstrap values. Hs, *Homo sapiens*; Dm, *Drosophila melanogaster*; Tg, *Toxoplasma gondii*; Pf, *Plasmodium falciparum*; Sc, *Saccharomyces cerevisiae*; BESB, *Besnoitia besnoiti*; Bd, *Babesia duncani*; Bb, *Babesia bigemina*; BBOV, *Babesia bovis*; Bm, *Babesia microti*; Ta, *Theileria annulata*; Tp, *Theileria parva*

Chromosome distribution and interspecies collinearity analysis of the identified putative KMTs and JHDMs

Chromosome distribution analysis of the screened putative KMTs and JHDMs in the six Piroplasm species based on the GFF genome annotation files revealed that the identified genes were mainly concentrated on three to five chromosomes in each parasite's genome (Fig. 2A-F). The genes identified in *B. duncani*, *B. bovis* and *T. annulata* were mainly distributed on 3 chromosomes, in *B. bigemina* on 5 chromosomes and in *B. microti* and *T. parva* on 4 chromosomes.

To further explore the synteny relationships of the putative KMTs and the JHDMs among *B. duncani*, *B. bigemina*, *B. bovis*, *B. microti*, *T. annulata* and *T. parva*, we conducted an interspecies collinearity analysis. As shown in Fig. 2G, B. *duncani* and *B. bovis* share six pairs of collinear putative KMT genes and one pair of collinear JHDM genes; two pairs of collinear putative KMT genes were found between *B. duncani* and *B. microti*; seven putative KMT and one JHDM homologous genes were found between *B. duncani* and *B. bigemina*, whereas, *B. duncani* and *T. annulata* share five putative KMT and one JHDM homologous genes; besides, five putative KMT and two JHDM homologous genes were identified between *B. duncani* and *T. parva* and *T.parva* and *T. annulata*, respectively.

Conserved motif, gene architecture and domain analysis of the identified putative KMTs and JHDMs

Based on the MEME search, the conserved motifs and the corresponding distributions in the putative KMTs and JHDMs were analyzed. A total of ten conserved motifs were retrieved for the putative KMTs and JHDMs, separately. Notably, the distribution and constitution of the conserved motifs in the putative KMTs vary significantly. Generally, proteins belonging to the same KMT subfamily have similar motif constitutions and distributions. Noteworthily, all of the identified putative KMTs have a motif 1 sequence that contains a core "ELxFDY", an AdoMet binding and catalytic site (Fig. 3A). Additionally, motif 2, with a "RFINHSCxPN" core, and motif 3, with "GxG" and "YxG" cores, were distributed on most of the identified putative KMTs. "RFINHSCxPN", "GxG" and "YxG" are also canonical AdoMet catalytic motifs present in the majority of HKMTs from different species [25, 35, 40]. Another thing worth noting is that BdJmjC2, BbJmjC1, BBOVJmjC1, BmJmjC1, TaJmjC2 and TpJmjC2 share a similar composition and distribution of conserved motifs, however, BdJmjC1 has no common motifs (Fig. 3B). What's more, JHDM motifs 1 and 2, which contain "HxE/Ex$_n$H" Fe (II) and "N and K" α-KG binding sites, were highly conserved. The amino acid sequences of the conserved motifs essential for enzyme activity in the identified putative KMTs and JHDMs are shown as sequence logos (Fig. 4).

Gene structure exploration of the CDS, UTR and intron in the SET domain and JmjC domain gene families was carried out based on the genome annotation file (GFF). According to the gene structure analysis results, the number of exons in the SET gene family members fluctuated considerably (Fig. 3A). For example, *BBOVSET7* has 15 exons, while nine of the putative KMTs have only one exon. Interestingly, UTRs were found in the six putative KMT genes of *B. bovis*. For the JmjC gene family, the exon number of each member also varied drastically, ranging between 4 (*BdJmjC1*) and 12 (*TaJmjC2* and *TpJmjC2*) (Fig. 3B).

The functional conserved domains of the identified putative KMTs and JHDMs were obtained by a conserved domain search in the NCBI-CDD database. As shown in Fig. 3A, the domain constitutions in the same subfamily are obviously conserved. Among these 38 putative KMTs, with the exception of TaSETup3, additional conserved domains were found only in SETD1 family members, and all other subfamily members contained only one conserved SET domain. On the other hand, except for BdJmjC1 and TpJmjC1, all the identified JHDMs also contain a JmjN domain in addition to a JmjC domain. Moreover, a zf-C5HC2 domain was found to exist in BmJmjC1 and TaJmjC2 (Fig. 3B).

Gene expression profile of the putative KMTs and JHDMs in *B. duncani*

To figure out the gene expression patterns of the putative KMTs and JHDMs in *B. duncani*, we conducted real-time qPCR to determine the relative expression levels of these genes at different developmental stages. All the amplification reactions were performed in parallel in three duplicates. The primers, reaction systems and amplification conditions for RT–qPCR used in our study are listed in Tables S3 and S4, respectively. Meanwhile, the detailed information on the S1/S2/S3 stage samples and the results of relative expression levels as well as the statistical estimates are shown separately in supplementary Table S5 and S6. According to the heatmap of the relative gene expression levels (Fig. 5A), the expression patterns of the putative KMTs and the JHDMs varied significantly at different developmental stages. The majority of the putative KMT and JHDM genes exhibited increased expression with parasite development, with the exception of *BdSET1*, whose expression decreased as *B. duncani* parasites developed from S1 to S2 and increased from S2 to S3. These results imply that the identified putative KMT

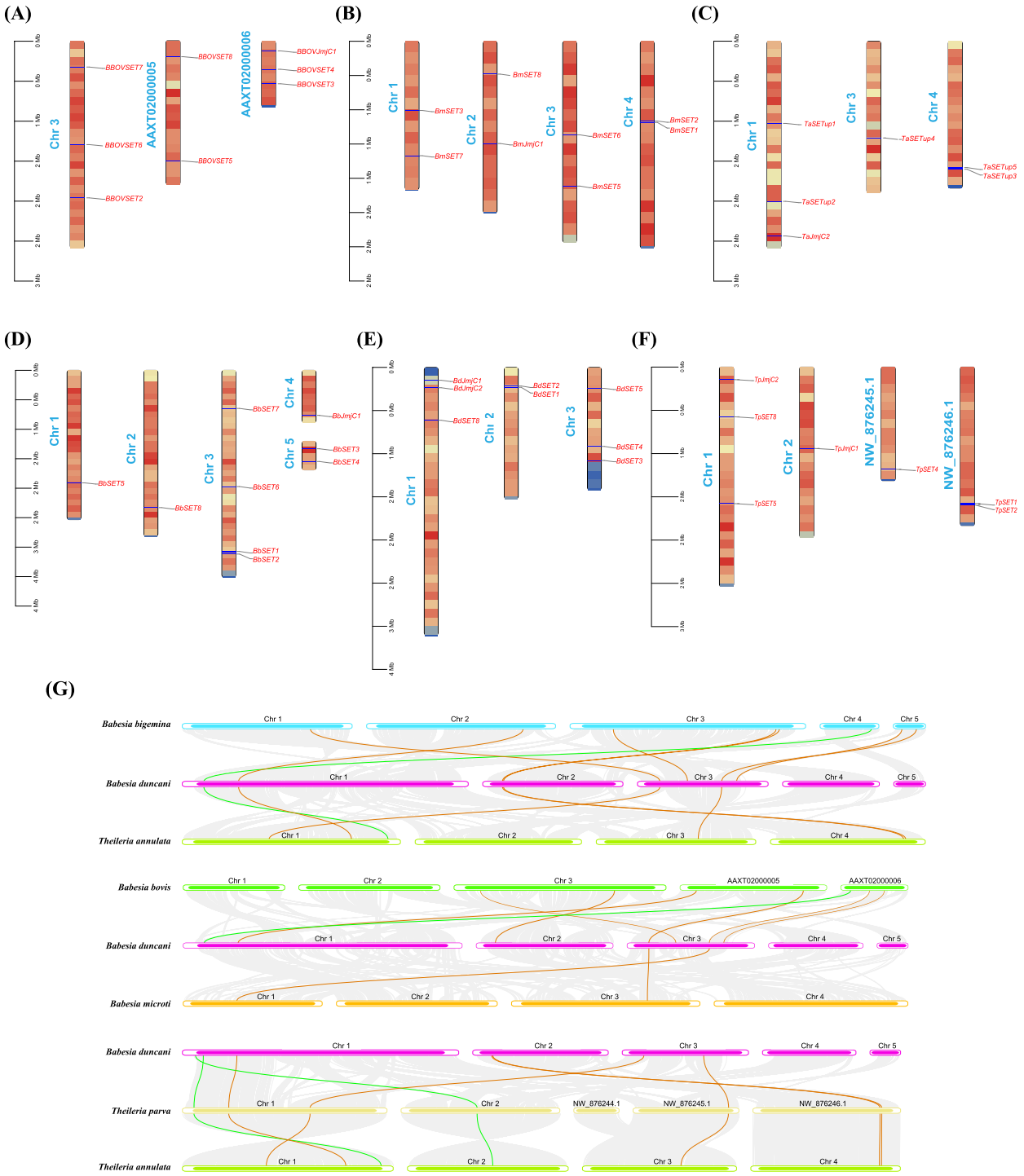

Fig. 2 Chromosomal distributions (**A** to **F**) and interspecies collinearity analysis (**G**) of putative KMT and JHDM genes. Panels **A** to **F** are the chromosomal maps of the putative KMTs and JHDMs in the six piroplasm genomes: *Babesia bovis* (**A**), *Babesia microti* (**B**), *Theileria annulata* (**C**), *Babesia bigemina* (**D**), *Babesia duncani* (**E**) and *Theileria parva* (**F**). The upper part of (**G**) indicates the interspecies collinearity relationship of putative KMT and JHDM genes between *Babesia bigemina*, *Babesia duncani* and *Theileria annulata*, while the middle part indicates the interspecies relationship of putative KMT and JHDM genes between *Babesia bovis*, *Babesia duncani* and *Babesia microti*; the lower part indicates the interspecies relationship of putative KMT and JHDM genes between *Babesia duncani*, *Theileria parva* and *Theileria annulata*. The yellow lines indicate the collinearity relationship of putative KMT genes between species, and the green lines indicate the collinearity relationship of putative JHDM genes between species

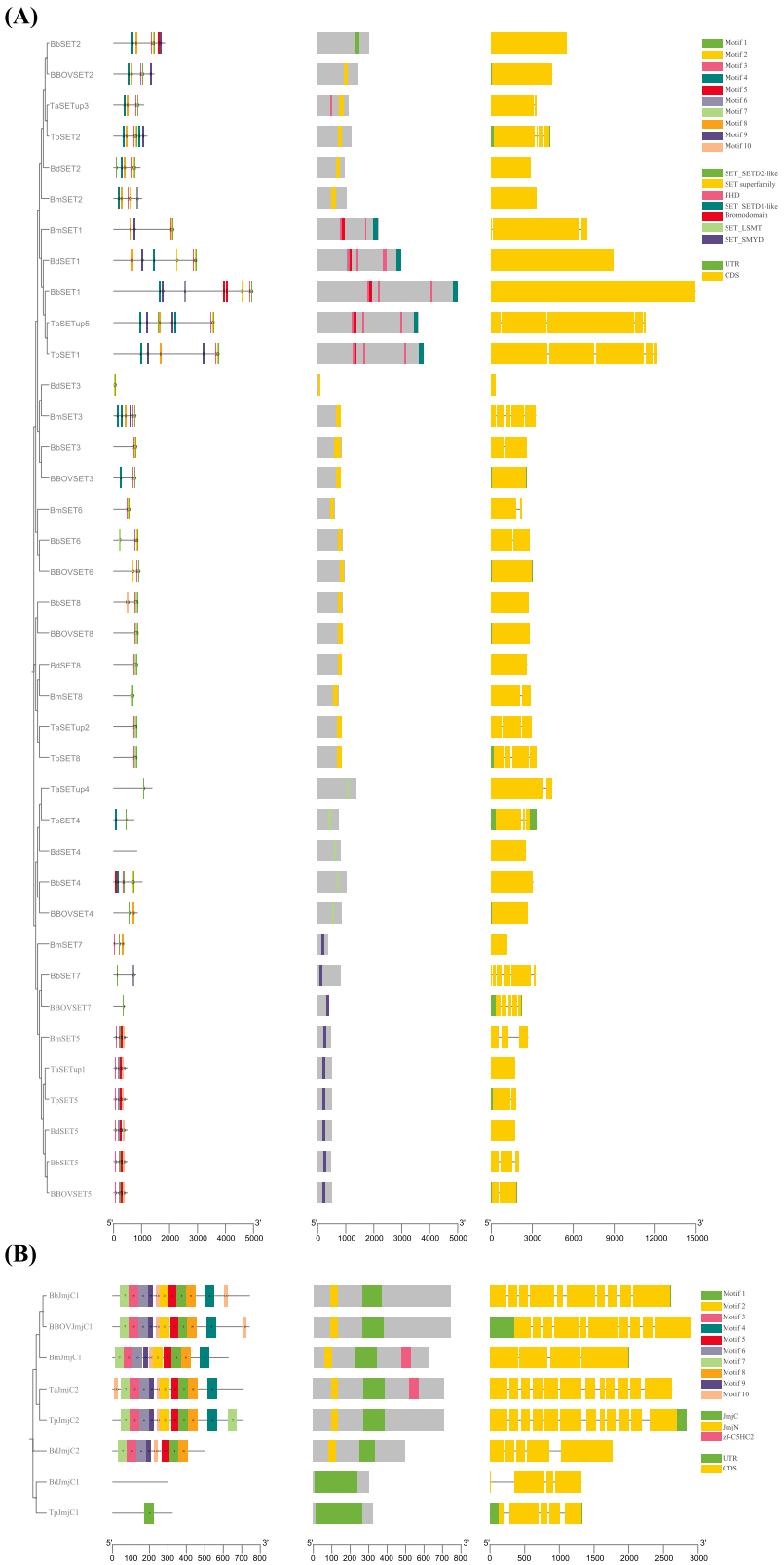

Fig. 3 Conserved motif (left), domain (middle) and gene structure (right) analysis of putative KMTs (**A**) and JHDMs (**B**) in *Babesia duncani*, *Babesia bigemina*, *Babesia bovis*, *Babesia microti*, *Theileria annulata* and *Theileria parva*

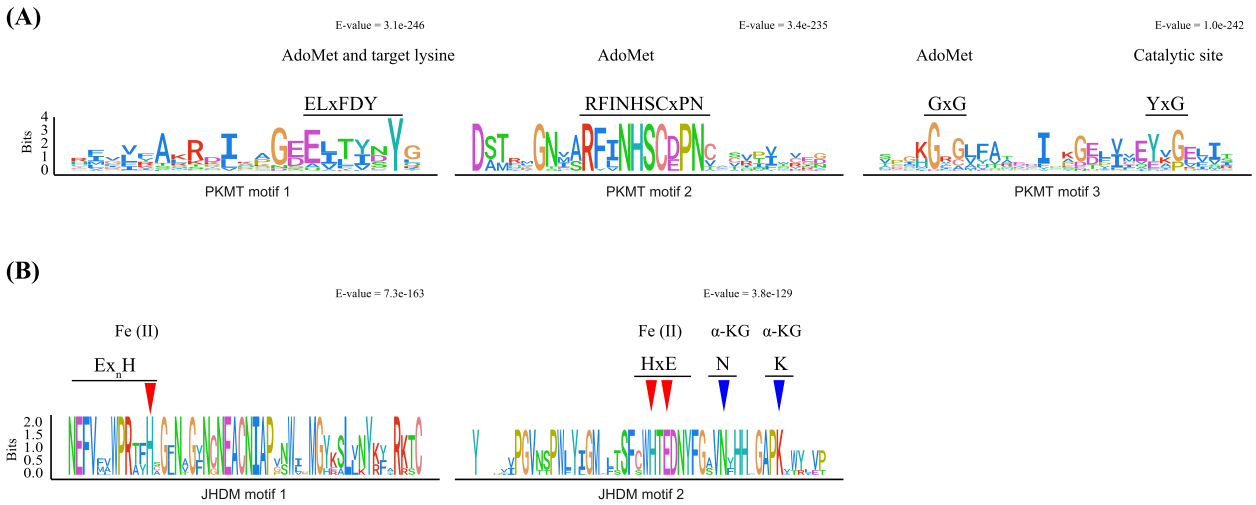

Fig. 4 The sequence logo of the conserved motifs found in the putative KMTs (**A**) and JHDMs (**B**) in *Babesia duncani*, *Babesia bigemina*, *Babesia bovis*, *Babesia microti*, *Theileria annulata* and *Theileria parva*

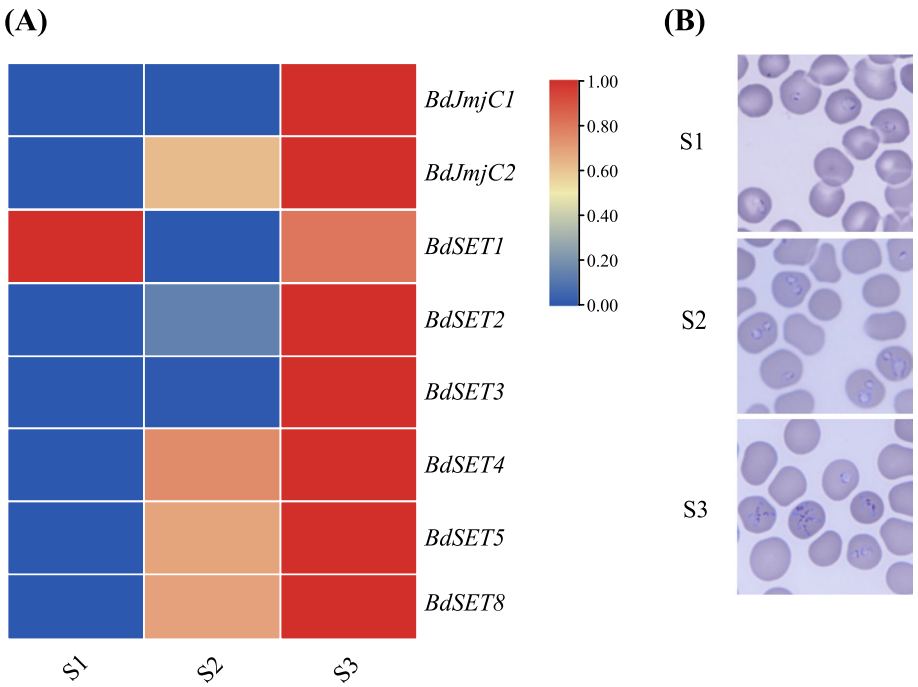

Fig. 5 Expression profiles of the putative KMT and JHDM genes at different developmental stages in *Babesia duncani*. **A** Heatmap of the relative expression levels of the putative KMT and JHDM genes in S1-, S2- and S3-stage *Babesia duncani*. **B** Images of S1, S2 and S3 intraerythrocytic stages of *Babesia duncani* from Giemsa-stained thin blood smears

and JHDM genes may be involved in the intraerythrocytic development of *B. duncani*, especially BdSET1 which may be a crucial regulator of stage transition.

Discussion

Histone methylation plays an essential role in various biological processes in Apicomplexa parasites, including

transcriptional regulation, chromatin remodeling, parasite-host interactions, parasite differentiation and pathogenicity [22, 25, 42, 43]. HKMTs and JHDMs are the "writers" and "erasers" of histone methylation, respectively, and are critical for maintaining dynamic changes in histone methylation levels. The widely studied functions and evolutionary history of the members of the HKMT and JHDM families in several Apicomplexa parasites, including *P. falciparum* [22, 35, 44, 45], *T. gondii* [36] and *C. parvum* [25], have stimulated our interest in the identification and characterization of the SET domain-containing or JmjC domain-containing gene families in the human pathogenic genus *Babesia*, such as *B. microti* and *B. duncani*, and in piroplasms of veterinary importance such as *B. bovis*, *B. bigemina*, *T. annulata* and *T. parva*.

In the current study, we conducted genome-wide identification and characterization of SET domain-containing KMTs and JHDMs in *B. duncani*, *B. bovis*, *B. bigemina*, *B. microti*, *T. annulata* and *T. parva*. A total of 38 putative KMT and eight JHDM genes were obtained, and SMART confirmed the presence of the SET domain and JmjC domain in each putative KMT and JHDM, respectively. However, the number of putative KMTs and JHDMs in the *B. microti*, *B. duncani*, *B. bovis* and *B. bigemina* genomes is close to that in the *P. falciparum* [35] and *C. parvum* [25] genomes, much less than that in *H. sapiens* (HKMTs > 50 and HKDMs > 30) [46], which may be due to the relatively compact size of the genome of Apicomplexa parasites (genome size of *B. duncani* 10.4 Mb, *B. bigemina* 13.8 Mb, *B. bovis* 8.2 Mb, *B. microti* 6.4 Mb, *T. annulata* 8.4 Mb, *T. parva* 8.3 Mb, *P. falciparum* 23.3 Mb and *C. parvum* 9.1 Mb, whereas *H. sapiens* 3.1 Gb) and demonstrates the importance of the HKMT and JHDM gene families in Apicomplexa parasite evolution. The phylogenetic tree revealed that the 38 putative KMTs can be grouped into eight distinct subfamilies: SETD1, SETD2, SETD8, SVU39, SET7/9, SMYD, LSMT and others (a clade distinct from other known HKMT subfamilies). In *T. gondii*, TgAKMT can affect parasite motility, invasion and parasite egress by methylating non-histone proteins, and when TgAKMT is knocked out, parasite motility is inhibited and invasion and parasite egress are reduced [23, 36, 47]. Putative KMTs (BdSET5, BBOVSET5, BbSET5, BmSET5, TaSETup1 and TpSET5) that cluster with TgAKMT have been identified in each of these six Apicomplexan piroplasm genomes, and these genes are likely involved biological processes similar to those of TgAKMT. Interestingly, in the study by Cheeseman et al., TaSETup1 showed the ability to methylate H3K18 and may be involved in the regulation of stage differentiation in *T. annulata* [42]. These findings indicate that putative KMTs clustering with TgAKMT may be able to catalyze both non-histone and histone substrates to exert effects on parasite behavior. Since AKMT (Apicomplexa lysine methyltransferase) is a methyltransferase that does not exist in mammals but only in Apicomplexa parasites, investigating its mechanism in parasite development and pathogenesis could help develop new therapeutic strategies to control parasites. In addition, in *P. falciparum*, PfSET2 regulates *var* gene expression by modulating H3K36me3 levels on *var* genes, and in the absence of PfSET2, all *var* genes are expressed [22, 48, 49]. In this study, a SETD2 HKMT homologue was found in the genomes of each of the six piroplasm species. Future research to confirm whether these genes are involved in modulating the expression of var antigens in these six piroplasm strains, as they are in *P. falciparum*, will provide some theoretical support for the development of vaccines against these parasites. Moreover, we did not observe any intraspecies collinearity between these screened genes (data not shown), indicating that no duplicate events of these methylation-related genes occurred during evolution. Importantly, interspecies collinearity analysis of piroplasm species also unraveled the significance of the HKMT and JHDM genes in species evolution.

Due to the limited number of transcription factors in Apicomplexa protozoan genomes, other epigenetic regulatory mechanisms, such as histone lysine/arginine methylation or acetylation may also contribute greatly to protozoan development [43, 50, 51]. Previous studies have demonstrated that histone methylation levels are involved in orchestrating the cell differentiation of Apicomplexa parasites and their complex life cycle [25, 42, 52]. Accordingly, dynamic changes in histone lysine methylation levels usually occur together with alterations in gene expression throughout the parasite development stages [44, 53–55]. Therefore, we analyzed the expression patterns of the putative KMTs and JHDMs in different developmental stages of *B. duncani*. According to the relative expression levels of the genes identified by RT–qPCR (Fig. 5), the putative KMT and JHDM genes exhibit distinct expression profiles in different intraerythrocytic developmental stages. The expression level of BdSET1 gradually decreased with parasite development from S1 to S2, and increased as *B. duncani* parasites developed from S2 to S3. BdSET1 is a SETD1 superfamily member supported by a high bootstrap value according to the phylogenetic tree constructed from well-studied HKMTs (Fig. 1A). Furthermore, BdSET1 possesses four additional PHDs and one bromodomain, similar in domain number and constitution to other SETD1 family members, such as BmSET1, BbSET1 TaSETup5 and TpSET1 (Fig. 3A). The PHD and bromodomain can bind to the H3K4 site and are essential for the HKMT activity of SETD1 family members [56–58]. Therefore, we speculate that BdSET1

may be able to catalyze H3K4 to form mono-, di- or trimethylated H3K4. Besides, H3K4 methylation is an active marker of transcription and several studies have demonstrated that the methylation level of H3K4 is associated with parasite life cycle progression [58]. These findings raise the possibility that BdSET1 might be a critical regulator of *B. duncani* parasite development. However, more well-designed studies should be performed to support this speculation.

Conclusions

In general, this study could help the scientific community acquire more basic information on the HKMTs and JHDMs of human pathogenic and veterinary important Piroplasm parasites and lay a theoretical foundation for future works on the mechanisms of histone lysine methylation regulation in Apicomplexa babesia parasite differentiation.

Materials and methods

Identification of putative KMTs and JHDMs

The SET motifs of several well-studied histone lysine methyltransferases (shown in supplementary Table S1) from different species, including human, Drosophila, and Apicomplexa protozoans like *Toxoplasma gondii* and *Plasmodium falciparum* [25], were used as queries with BLASTp algorithm (https://blast.ncbi.nlm.nih.gov/) to search for potential SET domain-containing KMTs in *B. duncani* (accession number: GCA_028658345.1), *B. microti* (GCF_000691945.2), *B. bigemina* (GCF_000981445.1), *B. bovis* (GCF_000165395.2), *T. annulata* (GCF_000003225.4) and *T. parva* (GCF_000165365.1) genomes. Parallelly, the amino acid sequences of the JumonjiC (JmjC) domain of representative human histone lysine demethylases [41] (Table S2) were also subjected to a search for putative JHDMs in the same genome sets. Moreover, the presence of SET domain in putative KMTs and the presence of JmjC domain in putative JHDMs of these six species were confirmed using the Simple Modular Architecture Research Tool (SMART, http://smart.embl.de/). The basic characteristics of the identified proteins, including molecular weight (kDa) and isoelectric point (PI), were obtained by the ExPASy website tool (https://prosite.expasy.org/). Besides, Euk-mPLoc 2.0 online software [59] (http://www.csbio.sjtu.edu.cn/bioinf/euk-multi-2/) was used to predict the subcellular localization of the putative KMTs and JHDMs.

Phylogenetic analysis

Multiple sequence alignment was performed using the Megalign tool by the Clustal W algorithm imbedded in MEGA 7 software (Molecular Evolutionary Genetics Analysis Version 7.0) to compare the conserved SET domain or JmjC domain sequences of the identified proteins with the representative HKMTs or JHDMs listed in Tables S1 and S2, respectively. Subsequently, phylogenetic tree files for the SET domain or the JmjC domain sequences of these proteins were generated using MEGA 7 with the maximum likelihood (ML) algorithm due to its relatively higher accuracy and faster computing speed. The reliability was evaluated by 1000 bootstrap replications. Thereafter, visualization and beautification of the tree files were performed on the R-project platform using the "ggplot2", "treeio" and "ggtree" packages [60, 61].

Chromosomal distribution and interspecies collinearity analysis

The genome sequence (FASTA) and annotation (GFF) files of the six piroplasm strains were downloaded from GenBank. The chromosome length and gene distribution information obtained from the genome annotation file (GFF) and the gene IDs of the identified putative KMTs and JHDMs were visualized with the "Gene Location Visualize from GTF/GFF" program imbedded in TBtools software. The interspecies collinearity relationships of the putative KMT and JHDM genes among *B. duncani*, *B. bovis*, *B. microti*, *B. bigemina*, *T. annulata* and *T. parva* were evaluated via the Multiple Collinearity Scan toolkit (MCScanX) (e-value threshold = 1e-10) and visualized via the Multiple Synteny Plot program in TBtools [62].

Conserved motif, architecture and gene structure analysis

The conserved motifs of putative KMTs or JHDMs of the six species were searched using the Multiple Em for Motif Elicitation (MEME) online website tool (https://meme-suite.org/meme/tools/meme) [63] with the parameters set to a maximum number of motifs of 10 and an optimal motif width of 6—50. The gene structure of putative KMTs and JHDMs, including CDSs, introns and UTRs, were predicted and visualized by TBtools using the corresponding genome annotation files of these species. The conserved domains of all the identified proteins were analyzed and searched with the NCBI Batch CD-search Tool (https://www.ncbi.nlm.nih.gov/Structure/bwrpsb/bwrpsb.cgi). Moreover, sequence logos for the conserved motif of the identified proteins were generated through a MEME search and visualized on the R-project platform using the "ggplot2" and "ggseqlogo" packages [64].

In vivo parasite culture and collection of merozoites at different developmental stages

A vial of *B. duncani* WA1 purchased from ATCC and cryopreserved in liquid nitrogen at Vector and Vector-Borne Diseases (VVBD) Laboratory, Lanzhou Veterinary Research Institute (LVRI) (CAAS Lanzhou, China) was

thawed quickly in a water bath at 37℃. Immediately, a 10-week-old female Golden Syrian hamster (Chales River Laboratories, Beijing, China) was inoculated with the whole vial of parasite via intraperitoneal injection. Parasitemia was monitored daily from day 5 post infection (p.i.) by thin blood smears stained with Giemsa prepared via lateral saphenous venipuncture through microscopic examination with a × 1000 oil-immersion lens. When the parasitemia increased to approximately 10%, the hamster was anesthetized with isoflurane (Orbiepharm, Qingdao, China) in an ABS Rodent Gas Anesthesia System (Yuyan Instruments Corporation, Shanghai) with consumption of isoflurane set at 5 ml/hour. The hamsters were then euthanized by collecting blood via cardiac puncture. Fresh infected blood was diluted in RPMI-1640 medium. Immediately following dilution, six 10-week-old female Golden Syrian hamsters (Chales River Laboratories, Beijing, China) were inoculated with diluted blood (2500 infected erythrocytes/500 μL/hamster). Thin blood smears were prepared and stained with Giemsa to monitor the parasite morphology daily after 5 dpi. Based on the parasite morphology within erythrocytes under microscopy and the intraerythrocytic cell division cycle of *Babesia* spp. proposed by Rezvani, et al. [65], the developmental stages of *B. duncani* could be artificially divided into several phases. Distinct morphologies (e.g. single-ring, double-ring and tetradic forms) could represent different developmental stages (named as S1/S2/S3 stages, respectively). In the early stages of infection, single-ring forms predominate (> 90%), and as the infection progresses, double-ring and tetradic forms progressively increase, and when double-ring forms predominate over tetradic forms, the developmental stage is assumed to be S2, whereas when tetradic forms predominate over single-ring forms, it can be considered to be S3. Hamsters were anesthetized and euthanized as aforementioned, and blood samples were collected in EDTA-K_2 anticoagulant vacuum tubes. Immediately thereafter, *B. duncani* merozoites were extracted from infected erythrocytes and purified as previously described [66].

Total RNA extraction, cDNA library establishment and real-time quantitative PCR (RT–qPCR)

For all merozoites at different developmental stages, 100 μl of purified merozoites was used to extract total RNA using TRIzol Reagent (Life Technologies) according to the manufacturer's instructions. After removing the potentially contaminating genomic DNA by a gDNA eraser kit (Takara), 1 μg of total RNA was reverse transcribed to establish a cDNA library using PrimScript™ RT reagent kit (Takara) in a 20 μl reaction. RT–qPCR was carried out on an Agilent Mx3005P instrument (Agilent Technologies) to determine the relative gene expression levels using a TB Green® Kit (Takara Bio USA, Inc.) in accordance with the manufacturer's instructions. A housekeeping gene of *B. duncani* HSP70 (BdWA1_003044) was used as the internal reference gene [42] and the relative expression levels of the identified putative KMTs and JHDMs were calculated using the $2^{-\Delta\Delta Ct}$ method [67]. The average relative expression of the putative KMT and JHDM genes at different developmental stages was visualized using the Heatmap Illustrator program embedded in TBtools software.

Abbreviations

SET	Su(var.)3–9 (Suppressor of variegation 3–9), E(Z) (Enhancer of zeste) and Trx(Trithorax)
JmjC	Jumonji C
HKMT	Histone lysine methyltransferase
JHDM	JmjC domain histone demethylases
me1	Monomethylated
me2	Dimethylated
me3	Trimethylated
SUV39	Suppressor of variegation 3–9
EZ	Enhancer of zeste
LSMT	Large subunit methyltransferase
SMYD	Su(Var)3–9, Enhancer-of-zeste and Trithorax (SET) and Myeloid, Nervy, and DEAF-1 (MYND)
LSD	Lysine specific demethylase
FAD	Flavin adenine dinucleotide
PHD	Plant homeodomain
PHF2/PHF8	PHD finger lysine-specific demethylase 2/8
JARID	Jumonji/ARID domain-containing protein
UTX/UTY	Ubiquitously transcribed TPR gene on X/Y chromosome
MEME	Multiple Em for Motif Elicitation
UTR	Untranslated region
SMART	Simple Modular Architecture Research Tool
PCR	Polymerase chain reaction

Supplementary Information

The online version contains supplementary material available at https://doi.org/10.1186/s12864-024-10731-2.

Supplementary Material 1.

Supplementary Material 2.

Supplementary Material 3.

Supplementary Material 4.

Supplementary Material 5.

Supplementary Material 6.

Acknowledgements

We would like to thank all the members of Vector and Vector-Borne Diseases (VVBD) Laboratory who helped with this study but are not listed in this paper.

Authors' contributions

CGY, GQG, HY and QDL designed and planned this study. QDL, SDZ, JMW and ZEL conducted the experiments and performed the data analysis. QDL and SDZ drafted the manuscript. CGY, GQG, JMW and HY critically revised the paper. All the authors have read the paper and agree to its publication.

Funding

This work was financially supported by grants from the National Key Research and Development Program of China (2022YFD1800200), the National Nature Science Foundation of China (NO. 31972701), the Science Fund for Creative Research Groups of Gansu Province, China (22JR5RA024), Natural Science Foundation of Gansu, China (22JR5RA031), the Agricultural Science and

Technology Innovation Program, China (ASTIP) (CAAS-ASTIP-2016-LVRI), NBCIS (CARS-37), National Parasitic Resources Center, China (NPRC-2019–194-30), the Leading Fund of Lanzhou Veterinary Research Institute, China (LVRI-SZJJ-202105), and the hatching program of the State Key Laboratory for Animal Disease Control and Prevention, China (SKLVEB2021CGQD02 and SKLADCP2023HP04).

Availability of data and materials

All data generated or analysed during this study are included in this article and its supplementary information files. The genomic data used in this study are available in the NCBI database (https://www.ncbi.nlm.nih.gov/datasets/genome/; accession numbers: GCA_028658345.1 for *B. duncani*; GCF_000691945.2 for *B. microti*; GCF_000981445.1 for *B. bigemina*; GCF_000165395.2 for *B. bovis*; GCF_000003225.4 for *T. annulata* and GCF_000165365.1 for *T. parva*).

Declarations

Ethics approval and consent to participate

All of the animal experimental protocols were approved by the Animal Ethics Committee of Lanzhou Veterinary Research Institute, Chinese Academy of Agricultural Sciences (Approval No. LVRIAEC-2023–03). All of the experiments were carried out under the Ethical Procedures and Guidelines of People's Republic of China.

Consent for publication

Not applicable.

Competing interests

The authors declare no competing interests.

Received: 7 May 2024 Accepted: 21 August 2024
Published: 26 August 2024

References

1. Zanet S, Trisciuoglio A, Bottero E, de Mera IG, Gortazar C, Carpignano MG, Ferroglio E. Piroplasmosis in wildlife: *Babesia* and *Theileria* affecting free-ranging ungulates and carnivores in the Italian Alps. Parasit Vectors. 2014;7:70.
2. Tait A, Hall FR. *Theileria annulata*: control measures, diagnosis and the potential use of subunit vaccines. Rev Sci Tech (International Office of Epizootics). 1990;9(2):387–403.
3. Malgwi SA, Ogunsakin RE, Oladepo AD, Adeleke MA, Okpeku M. A forty-year analysis of the literature on *Babesia* Infection (1982–2022): a systematic bibliometric approach. Int J Environ Res Public Health. 2023;20(12):6156.
4. Lim PL, Chavatte JM, Vasoo S, Yang J. Imported human babesiosis, Singapore, 2018. Emerg Infect Dis. 2020;26(4):826–8.
5. Scott JD. First record of locally acquired human babesiosis in Canada caused by *Babesia duncani*: a case report. SAGE Open Med Case Rep. 2017;5:2050313X17725645.
6. Montero E, Folgueras M, Rodriguez-Pérez M, Pérez-Ls L, Díaz-Arias J, Meana M, Revuelta B, Haapasalo K, Collazos J, Asensi V, et al. Retrospective study of the epidemiological risk and serological diagnosis of human babesiosis in Asturias, Northwestern Spain. Parasit Vectors. 2023;16(1):195.
7. Hong SH, Kim SY, Song BG, Rho JR, Cho CR, Kim CN, Um TH, Kwak YG, Cho SH, Lee SE. Detection and characterization of an emerging type of *Babesia* sp. similar to *Babesia motasi* for the first case of human babesiosis and ticks in Korea. Emerg Microbes Infect. 2019;8(1):869–78.
8. Jia N, Zheng YC, Jiang JF, Jiang RR, Jiang BG, Wei R, Liu HB, Huo QB, Sun Y, Chu YL, et al. Human babesiosis caused by a *Babesia crassa*-like pathogen: a case series. Clin Infect Dis : an official publication of the Infectious Diseases Society of America. 2018;67(7):1110–9.
9. Calvopiña M, Montesdeoca-Andrade M, Bastidas-Caldes C, Enriquez S, Rodríguez-Hidalgo R, Aguilar-Rodríguez D, Cooper P. Case report: first report on human infection by tick-borne *Babesia bigemina* in the Amazon region of Ecuador. Front Public Health. 2023;11:1079042.
10. Huang L, Sun Y, Huo DD, Xu M, Xia LY, Yang N, Hong W, Nie WM, Liao RH, Zhang MZ, et al. Successful treatment with doxycycline monotherapy for human infection with *Babesia venatorum* (Babesiidae, Sporozoa) in China: a case report and proposal for a clinical regimen. Infect Dis Poverty. 2023;12(1):67.
11. Gaffar FR, Franssen FF, de Vries E. *Babesia bovis* merozoites invade human, ovine, equine, porcine and caprine erythrocytes by a sialic acid-dependent mechanism followed by developmental arrest after a single round of cell fission. Int J Parasitol. 2003;33(14):1595–603.
12. Foster E, Maes SA, Holcomb KM, Eisen RJ. Prevalence of five human pathogens in host-seeking Ixodes scapularis and Ixodes pacificus by region, state, and county in the contiguous United States generated through national tick surveillance. Ticks Tick Borne Dis. 2023;14(6):102250.
13. Pal AC, Renard I, Singh P, Vydyam P, Chiu JE, Pou S, Winter RW, Dodean R, Frueh L, Nilsen AC, et al. *Babesia duncani* as a model organism to study the development, virulence, and drug susceptibility of intraerythrocytic parasites in vitro and in vivo. J Infect Dis. 2022;226(7):1267–75.
14. Mamoun CB, Allred DR. Babesiosis. eLS. 2018:1–8.
15. Zhou X, Xia S, Huang JL, Tambo E, Zhuge HX, Zhou XN. Human babesiosis, an emerging tick-borne disease in the People's Republic of China. Parasit Vectors. 2014;7:509.
16. Thomford JW, Conrad PA, Boyce WM, Holman PJ, Jessup DA. Isolation and in vitro cultivation of *Babesia* parasites from free-ranging desert bighorn sheep (Ovis canadensis nelsoni) and mule deer (Odocoileus hemionus) in California. J Parasitol. 1993;79(1):77–84.
17. Bosman A-M, Penzhorn BL, Brayton KA, Schoeman T, Oosthuizen MC. A novel *Babesia sp.* associated with clinical signs of babesiosis in domestic cats in South Africa. Parasit Vectors. 2019;12(1):138.
18. Gabrielli S, Otašević S, Ignjatović A, Savić S, Fraulo M, Arsić-Arsenijević V, Momčilović S, Cancrini G. Canine Babesioses in Noninvestigated Areas of Serbia. Vector Borne Zoonotic Dis (Larchmont, NY). 2015;15(9):535–8.
19. Chen X-R, Ye LI, Fan J-W, Li C, Tang F, Liu WEI, Ren L-Z, Bai J-Y. Detection of Kobe-type and Otsu-type *Babesia microti* in wild rodents in China's Yunnan province. Epidemiol Infect. 2017;145(13):2704–10.
20. Gao ZH, Huang TH, Jiang BG, Jia N, Liu ZX, Shao ZT, Jiang RR, Liu HB, Wei R, Li YQ, et al. Wide distribution and genetic diversity of *Babesia microti* in small mammals from Yunnan Province, Southwestern China. PLoS Negl Trop Dis. 2017;11(10):e0005898.
21. Akinyi MY, Tung J, Jeneby M, Patel NB, Altmann J, Alberts SC. Role of grooming in reducing tick load in wild baboons (Papio cynocephalus). Anim Behav. 2013;85(3):559–68.
22. Jiang L, Mu J, Zhang Q, Ni T, Srinivasan P, Rayavara K, Yang W, Turner L, Lavstsen T, Theander TG, et al. PfSETvs methylation of histone H3K36 represses virulence genes in *Plasmodium falciparum*. Nature. 2013;499(7457):223–7.
23. Heaslip AT, Nishi M, Stein B, Hu K. The motility of a human parasite, *Toxoplasma gondii*, is regulated by a novel lysine methyltransferase. PLoS Pathog. 2011;7(9):e1002201.
24. Bohaliga GAR, Johnson WC, Taus NS, Hussein HE, Bastos RG, Suarez CE, O'Connor R, Ueti MW. Identification of a putative methyltransferase gene of *Babesia bigemina* as a novel molecular biomarker uniquely expressed in parasite tick stages. Parasit Vectors. 2018;11(1):480.
25. Sawant M, Benamrouz-Vanneste S, Meloni D, Gantois N, Even G, Guyot K, Creusy C, Duval E, Wintjens R, Weitzman JB, et al. Putative SET-domain methyltransferases in *Cryptosporidium parvum* and histone methylation during infection. Virulence. 2022;13(1):1632–50.
26. Kaur P, Shankar E, Gupta S. EZH2-mediated development of therapeutic resistance in cancer. Cancer Lett. 2024;586:216706.
27. de Oliveira Filho RS, de Oliveira DA, Nisimoto MM, Marti LC. A review of advanced cutaneous melanoma therapies and their mechanisms, from immunotherapies to lysine histone methyl transferase inhibitors. Cancers. 2023;15(24):5751.
28. Rao H, Liu C, Wang A, Ma C, Xu Y, Ye T, Su W, Zhou P, Gao WQ, Li L, et al. SETD2 deficiency accelerates sphingomyelin accumulation and promotes the development of renal cancer. Nat Commun. 2023;14(1):7572.
29. Zheng X, Luo Y, Xiong Y, Liu X, Zeng C, Lu X, Wang X, Cheng Y, Wang S, Lan H, et al. Tumor cell-intrinsic SETD2 inactivation sensitizes cancer cells to immune checkpoint blockade through the NR2F1-STAT1 pathway. J Immunother Cancer. 2023;11(12):e007678.
30. Ngwa CJ, Kiesow MJ, Orchard LM, Farrukh A, Llinás M, Pradel G. The G9a histone methyltransferase inhibitor BIX-01294 modulates gene

expression during *Plasmodium falciparum* gametocyte development and transmission. Int J Mol Sci. 2019;20(20):5087.
31. Chan A, Dziedziech A, Kirkman LA, Deitsch KW, Ankarklev J. A histone methyltransferase inhibitor can reverse epigenetically acquired drug resistance in the malaria parasite *Plasmodium falciparum*. Antimicrob Agents Chemother. 2020;64(6):e02021.
32. Steketee PC, Vincent IM, Achcar F, Giordani F, Kim DH, Creek DJ, Freund Y, Jacobs R, Rattigan K, Horn D, et al. Benzoxaborole treatment perturbs S-adenosyl-L-methionine metabolism in *Trypanosoma brucei*. PLoS Negl Trop Dis. 2018;12(5):e0006450.
33. Zuma AA, Santos JO, Mendes I, de Souza W, Machado CR, Motta MCM. Chaetocin-A histone methyltransferase inhibitor-Impairs proliferation, arrests cell cycle and induces nucleolar disassembly in *Trypanosoma cruzi*. Acta Trop. 2017;170:149–60.
34. Rodrigues JC, Attias M, Rodriguez C, Urbina JA, Souza W. Ultrastructural and biochemical alterations induced by 22,26-azasterol, a delta(24(25))-sterol methyltransferase inhibitor, on promastigote and amastigote forms of *Leishmania* amazonensis. Antimicrob Agents Chemother. 2002;46(2):487–99.
35. Cui L, Fan Q, Miao J. Histone lysine methyltransferases and demethylases in *Plasmodium falciparum*. Int J Parasitol. 2008;38(10):1083–97.
36. Pivovarova Y, Liu J, Lesigang J, Koldyka O, Rauschmeier R, Hu K, Dong G. Structure of a novel dimeric SET domain methyltransferase that regulates cell motility. J Mol Biol. 2018;430(21):4209–29.
37. Del Rizzo PA, Trievel RC. Substrate and product specificities of SET domain methyltransferases. Epigenetics. 2011;6(9):1059–67.
38. Qian C, Zhou MM. SET domain protein lysine methyltransferases: structure, specificity and catalysis. Cell Mol Life Sci CMLS. 2006;63(23):2755–63.
39. Tsukada Y, Fang J, Erdjument-Bromage H, Warren ME, Borchers CH, Tempst P, Zhang Y. Histone demethylation by a family of JmjC domain-containing proteins. Nature. 2006;439(7078):811–6.
40. Husmann D, Gozani O. Histone lysine methyltransferases in biology and disease. Nat Struct Mol Biol. 2019;26(10):880–9.
41. Klose RJ, Kallin EM, Zhang Y. JmjC-domain-containing proteins and histone demethylation. Nat Rev Genet. 2006;7(9):715–27.
42. Cheeseman K, Jannot G, Lourenço N, Villares M, Berthelet J, Calegari-Silva T, Hamroune J, Letourneur F, Rodrigues-Lima F, Weitzman JB. Dynamic methylation of histone H3K18 in differentiating *Theileria* parasites. Nat Commun. 2021;12(1):3221.
43. Pain A, Renauld H, Berriman M, Murphy L, Yeats CA, Weir W, Kerhornou A, Aslett M, Bishop R, Bouchier C, et al. Genome of the host-cell transforming parasite *Theileria annulata* compared with *T. parva*. Science. 2005;309(5731):131–3.
44. Chen PB, Ding S, Zanghì G, Soulard V, DiMaggio PA, Fuchter MJ, Mecheri S, Mazier D, Scherf A, Malmquist NA. *Plasmodium falciparum* PfSET7: enzymatic characterization and cellular localization of a novel protein methyltransferase in sporozoite, liver and erythrocytic stage parasites. Sci Rep. 2016;6:21802.
45. Kishore SP, Stiller JW, Deitsch KW. Horizontal gene transfer of epigenetic machinery and evolution of parasitism in the malaria parasite *Plasmodium falciparum* and other apicomplexans. BMC Evol Biol. 2013;13:37.
46. Cole CG, McCann OT, Collins JE, Oliver K, Willey D, Gribble SM, Yang F, McLaren K, Rogers J, Ning Z, et al. Finishing the finished human chromosome 22 sequence. Genome Biol. 2008;9(5):R78.
47. Sivagurunathan S, Heaslip A, Liu J, Hu K. Identification of functional modules of AKMT, a novel lysine methyltransferase regulating the motility of *Toxoplasma gondii*. Mol Biochem Parasitol. 2013;189(1–2):43–53.
48. Sethumadhavan DV, Govindaraju G, Jabeena CA, Rajavelu A. *Plasmodium falciparum* SET2 domain is allosterically regulated by its PHD-like domain to methylate at H3K36. Biochim Biophys Acta. 2021;1864(10):194744.
49. Ukaegbu UE, Kishore SP, Kwiatkowski DL, Pandarinath C, Dahan-Pasternak N, Dzikowski R, Deitsch KW. Recruitment of PfSET2 by RNA polymerase II to variant antigen encoding loci contributes to antigenic variation in *P. falciparum*. PLoS Pathog. 2014;10(1):e1003854.
50. Han Z, Zheng Y, Shi Y, Chen F, Wu C, Wang L, Lu S, Li D, Guan X, He L, et al. Transcriptional variation in *Babesia gibsoni* (Wuhan isolate) between in vivo and in vitro cultures in blood stage. Parasit Vectors. 2023;16(1):268.
51. Wang J, Chen K, Yang J, Zhang S, Li Y, Liu G, Luo J, Yin H, Wang G, Guan G. Comparative genomic analysis of *Babesia duncani* responsible for human babesiosis. BMC Biol. 2022;20(1):153.
52. Harris CT, Tong X, Campelo R, Marreiros IM, Vanheer LN, Nahiyaan N, Zuzarte-Luís VA, Deitsch KW, Mota MM, Rhee KY, et al. Sexual differentiation in human malaria parasites is regulated by competition between phospholipid metabolism and histone methylation. Nat Microbiol. 2023;8(7):1280–92.
53. Coleman BI, Skillman KM, Jiang RHY, Childs LM, Altenhofen LM, Ganter M, Leung Y, Goldowitz I, Kafsack BFC, Marti M, et al. A *Plasmodium falciparum* histone deacetylase regulates antigenic variation and gametocyte conversion. Cell Host Microbe. 2014;16(2):177–86.
54. Li Y, Liew YJ, Cui G, Cziesielski MJ, Zahran N, Michell CT, Voolstra CR, Aranda M. DNA methylation regulates transcriptional homeostasis of algal endosymbiosis in the coral model aiptasia. Sci Adv. 2018;4(8):eaat2142.
55. Bougdour A, Braun L, Cannella D, Hakimi MA. Chromatin modifications: implications in the regulation of gene expression in *Toxoplasma gondii*. Cell Microbiol. 2010;12(4):413–23.
56. Ortiz G, Kutateladze TG, Fujimori DG. Chemical tools targeting readers of lysine methylation. Curr Opin Chem Biol. 2023;74:102286.
57. Wysocka J, Swigut T, Xiao H, Milne TA, Kwon SY, Landry J, Kauer M, Tackett AJ, Chait BT, Badenhorst P, et al. A PHD finger of NURF couples histone H3 lysine 4 trimethylation with chromatin remodelling. Nature. 2006;442(7098):86–90.
58. Salusso A, Zlocowski N, Mayol GF, Zamponi N, Rópolo AS. Histone methyltransferase 1 regulates the encystation process in the parasite *Giardia lamblia*. FEBS J. 2017;284(15):2396–409.
59. Chou KC, Shen HB. A new method for predicting the subcellular localization of eukaryotic proteins with both single and multiple sites: Euk-mPLoc 2.0. PloS One. 2010;5(4):e9931.
60. Wang LG, Lam TT, Xu S, Dai Z, Zhou L, Feng T, Guo P, Dunn CW, Jones BR, Bradley T, et al. Treeio: an R package for phylogenetic tree input and output with richly annotated and associated data. Mol Biol Evol. 2020;37(2):599–603.
61. Yu G, Lam TT, Zhu H, Guan Y. Two methods for mapping and visualizing associated data on phylogeny using Ggtree. Mol Biol Evol. 2018;35(12):3041–3.
62. Chen C, Wu Y, Li J, Wang X, Zeng Z, Xu J, Liu Y, Feng J, Chen H, He Y, et al. TBtools-II: A "one for all, all for one" bioinformatics platform for biological big-data mining. Mol Plant. 2023;16(11):1733–42.
63. Bailey TL, Elkan C. Fitting a mixture model by expectation maximization to discover motifs in biopolymers. Proc Int Conf Intell Syst Mol Biol. 1994;2:28–36.
64. Wagih O. ggseqlogo: a versatile R package for drawing sequence logos. Bioinformatics (Oxford, England). 2017;33(22):3645–7.
65. Rezvani Y, Keroack CD, Elsworth B, Arriojas A, Gubbels MJ, Duraisingh MT, Zarringhalam K. Comparative single-cell transcriptional atlases of *Babesia* species reveal conserved and species-specific expression profiles. PLoS Biol. 2022;20(9):e3001816.
66. Guan G, Moreau E, Liu J, Ma M, Rogniaux H, Liu A, Niu Q, Li Y, Ren Q, Luo J, et al. BQP35 is a novel member of the intrinsically unstructured protein (IUP) family which is a potential antigen for the sero-diagnosis of *Babesia* sp. BQ1 (Lintan) infection. Vet Parasitol. 2012;187(3–4):421–30.
67. Livak KJ, Schmittgen TD. Analysis of relative gene expression data using real-time quantitative PCR and the 2(-Delta Delta C(T)) method. Methods (San Diego, Calif). 2001;25(4):402–8.

Publisher's Note